Mio-First Comprehensive Exploration of Mercury's Space Environment: Mission Overview

Go Murakami, Hajime Hayakawa, Hiroyuki Ogawa, Shoya Matsuda, Taeko Seki, Yasumasa Kasaba, Yoshifumi Saito, Ichiro Yoshikawa, Masanori Kobayashi, Wolfgang Baumjohann, et al.

Space Science Reviews

Mio - First comprehensive exploration of Mercury's space environment: mission overview

--Manuscript Draft--

Manuscript Number:	
Full Title:	Mio - First comprehensive exploration of Mercury's space environment: mission overview
Article Type:	Vol xxx: The BepiColombo Mission to Mercury
Keywords:	BepiColombo, Mercury, Magnetosphere, Exosphere, Dust, Planetary environment
Corresponding Author:	Go Murakami Sagamihara, JAPAN
Corresponding Author Secondary Information:	
Corresponding Author's Institution:	
Corresponding Author's Secondary Institution:	
First Author:	Go Murakami
First Author Secondary Information:	
Order of Authors:	Go Murakami
	Hajime Hayakawa, Dr.
	Hiroyuki Ogawa, Dr.
	Shoya Matsuda, Dr.
	Taeko Seki
	Yasumasa Kasaba, Dr.
	Yoshifumi Saito, Dr.
	Ichiro Yoshikawa, Dr.
	Masanori Kobayashi, Dr.
	Wolfgang Baumjohann, Dr.
	Ayako Matsuoka, Dr.
	Hirotsugu Kojima, Dr.
	Satoshi Yagitani, Dr.
	Michel Moncuquet, Dr.
	Jan-Erik Wahlund, Dr.
	Dominique Delcourt, Dr.
	Masafumi Hirahara, Dr.
	Stas Barabash, Dr.
	Oleg Korablev, Dr.
	Masaki Fujimoto, Dr.
Order of Authors Secondary Information:	
Funding Information:	Institute of Space and Astronautical Science — Dr. Go Murakami

Abstract:	Mercury has a unique and complex space environment with its weak global magnetic field, intense solar wind, tenuous exosphere, and magnetospheric plasma particles. The first Mercury orbiter, MErcury Surface, Space ENvironment, GEochemistry, and Ranging (MESSENGER), was highly informative of the dynamic nature of Mercury's magnetosphere. However, due to the highly elliptical orbit with north-south asymmetry and limited capability for plasma measurements of the probe, many science questions raised by the MESSENGER mission remain unsolved. BepiColombo, a joint mission to Mercury by European Space Agency and Japan Aerospace Exploration Agency, will address these open questions using two spacecraft, Mio and Mercury Planetary Orbiter. Mio is a spin-stabilized spacecraft designed to investigate Mercury's space environment, with a powerful suite of plasma instruments, a spectral imager for the exosphere, and a dust monitor. Because of strong constraints on operations during its orbiting phase around Mercury, sophisticated observation and downlink plans are required in order to maximize science outputs. This paper gives an overview of the Mio spacecraft and its mission, operations plan, and data handling and archiving.

Mio－First comprehensive exploration of Mercury's space environment: mission overview

Go Murakami[a], Hajime Hayakawa[a], Hiroyuki Ogawa[a], Shoya Matsuda[a], Taeko Seki[a], Yasumasa Kasaba[b], Yoshifumi Saito[a], Ichiro Yoshikawa[c], Masanori Kobayashi[d], Wolfgang Baumjohann[e], Ayako Matsuoka[f], Hirotsugu Kojima[g], Satoshi Yagitani[h], Michel Moncuquet[i], Jan-Erik Wahlund[j], Dominique Delcourt[k], Masafumi Hirahara[l], Stas Barabash[m], Oleg Korablev[n], Masaki Fujimoto[a]

[a] Institute of Space and Astronautical Science, Japan Aerospace Exploration Agency, Sagamihara, Kanagawa 252-5210, Japan

[b] Planetary Plasma and Atmospheric Research Center, Graduate School of Science, Tohoku University, Sendai, Miyagi 980-8578, Japan

[c] Department of Complexity Science and Engineering, University of Tokyo, Kashiwa, Chiba 277-8561, Japan

[d] Planetary Exploration Research Center, Chiba Institute of Technology, 2-17-1, Tsudanuma, Narashino, Chiba 275-0016, Japan

[e] Space Research Institute, Austrian Academy of Sciences, Schmiedlstraße 6, 8042 Graz, Austria

[f] Data Analysis Center for Geomagnetism and Space Magnetism, Graduate School of Science, Kyoto University, Sakyo, Kyoto 606-8502, Japan

[g] Research Institute for Sustainable Humanosphere, Kyoto University, Uji, Kyoto 611-0011, Japan

[h] Advanced Research Center for Space Science and Technology, Kanazawa University, Kakuma-machi, Kanazawa 920-1192, Japan

[i] LESIA, Observatoire de Paris, Université PSL, CNRS, 5, Place Jules Janssen 92195 Meudon, France

[j] Swedish Institute of Space Physics, Box 537, SE-751 21 Uppsala, Sweden

[k] CNRS-Universite d'Orleans-CNES, Orleans 45071, France

[l] Institute of Space-Earth Environmental Research, Nagoya University, Nagoya, Aichi 464-8601 Japan

[m] Swedish Institute of Space Physics, Box 812, SE-981 28 Kiruna, Sweden

[n] IKI-RAS Space Research Institute of Russian Academy of Science, Profsoyuznaya St. 84/32, Moscow 117997, Russia

Corresponding author:
Go Murakami
go@stp.isas.jaxa.jp
Tel 81-50-3362-3622

Abstract

Mercury has a unique and complex space environment with its weak global magnetic field, intense solar wind, tenuous exosphere, and magnetospheric plasma particles. The first Mercury orbiter, MErcury Surface, Space ENvironment, GEochemistry, and Ranging (MESSENGER), was highly informative of the dynamic nature of Mercury's magnetosphere. However, due to the highly elliptical orbit with north-south asymmetry and limited capability for plasma measurements of the probe, many science questions raised by the MESSENGER mission remain unsolved. BepiColombo, a joint mission to Mercury by European Space Agency and Japan Aerospace Exploration Agency, will address these open questions using two spacecraft, Mio and Mercury Planetary Orbiter. Mio is a spin-stabilized spacecraft designed to investigate Mercury's space environment, with a powerful suite of plasma instruments, a spectral imager for the exosphere, and a dust monitor. Because of strong constraints on operations during its orbiting phase around Mercury, sophisticated observation and downlink plans are required in order to maximize science outputs. This paper gives an overview of the Mio spacecraft and its mission, operations plan, and data handling and archiving.

Keywords

Mercury; Magnetosphere; Exosphere; BepiColombo; Mercury Magnetospheric Orbiter (MMO); Mio;

1. Introduction

Mercury is the innermost planet in the Solar System and has a unique space environment. Mercury possesses a weak global magnetic field and is subject to the intense solar wind due to its proximity to the Sun (0.31-0.47 AU). In such conditions, Mercury formed a small but highly dynamic magnetosphere. Because of its small size and its proximity to the Sun, Mercury was unable to retain the bulk of its atmosphere but formed instead a tenuous exosphere, which is continuously refilled and eroded from the surface by interactions with solar winds, magnetospheric particles, and micro-meteoroid flux, etc. This complex system, characterized by surface–exosphere–magnetosphere–solar wind interactions, makes Mercury's space environment unique and an excellent science target for comparative study with Earth [Milillo et al., 2005]. In addition, recently many Earth-type exoplanets orbiting in habitable zones very close to cool stars (M-dwarfs) have been found [e.g., Gillon et al., 2017]. Such exoplanets are exposed to extreme stellar winds and ultraviolet radiations, and thus, investigating Mercury's complex system is key to understanding the extreme exoplanetary environment and its habitability conditions against strong stellar winds [e.g., Mura et al. 2011; Dong et al., 2017; 2018].

The first Mercury orbiter, MESSENGER (MErcury Surface, Space ENvironment, GEochemistry, and Ranging) [Solomon et al., 2007], explored this innermost region of the Solar System during 2011–2015 and provided a number of new findings. For example, Mercury's magnetosphere is much more

dynamic than had been predicted. Magnetic field measurements indicated Dungey cycles on Mercury with a period of a few minutes [Slavin et al., 2010]. MESSENGER detected many energetic electron events also with periodicities of a few minutes [Lawrence et al., 2015]. Electron precipitations at the nightside were discovered using X-ray and gamma-ray fluorescence [Lindsay et al., 2015; Dewey et al., 2018]. In addition, MESSENGER succeeded in measuring certain components of the exosphere, e.g., Na, Ca, and Mg [McClintock et al., 2008, 2009]. These measurements showed surprisingly constant year-to-year variations with strong seasonal dependence and no strong episodic events [Cassidy et al., 2015].

The MESSENGER mission addressed science aspects of Mercury using only one spacecraft and thus faced some constraints and limitations on investigating the environment. Its capability for plasma measurements was constrained because of the lack of low-energy electrons and plasma wave measurements and the limited field of view (FOV) of plasma particle measurements due to the three-axis attitude control of spacecraft. The MESSENGER orbit was highly elliptical with north-south asymmetry and detailed measurements in southern hemisphere were not achieved. Because of these constraints, many science questions remain unsolved even after the success of the MESSENGER mission (see details by Millilo et al. [this issue]).

The next Mercury exploration mission, BepiColombo, will address remaining open issues and will provide great improvements in knowledge through comprehensive complementary investigations. BepiColombo is an international joint project between European Space Agency (ESA) and Japan Aerospace Exploration Agency (JAXA) [Benkhoff et al., 2010], consisting of two spacecraft successfully launched on 20 October 2018 by an Ariane-5 launch vehicle. ESA's Mercury Planetary Orbiter (MPO) is a three-axis-stabilized, nadir-pointing module. MPO is dedicated to geology, planetary composition, inner structure, and the exosphere, and its low-eccentricity polar orbit will provide an excellent spatial resolution over the entirety of the planet's surface. The JAXA spacecraft "Mio"—Mercury Magnetospheric Orbiter (MMO)—is a spin-stabilized spacecraft to be placed in an eccentric polar orbit [Hayakawa et al., 2004; Yamakawa et al., 2008]. Mio is equipped to study the space environment of Mercury with its science instrument suite comprising a complete package of plasma instruments, a sodium exosphere spectral imager, and a dust monitor and is expected to extract essential elements of space plasma physics that become visible in Mercury's environment.

Mio will enable comparative studies of terrestrial planetary environments. Its main scientific objectives are to understand:

(1) the structure and origin of Mercury's magnetic field;

(2) the structure, dynamics, and physical processes of Mercury's magnetosphere;

(3) the structure, variation, and origin of Mercury's exosphere;

(4) the physical environment of inner heliosphere.

Table 1 describes the success criteria of the Mio mission.

As described in science target (4), the BepiColombo mission can analyze heliospheric physics in the inner Solar System in addition to conducting Mercury science. It will thus complement NASA's Parker Solar Probe, launched in 2018, which is currently orbiting the Sun (~0.05 AU at perihelion) [Fox et al., 2016], and ESA's Solar Orbiter [Müller et al., 2013], which will be launched in 2020 and will have a highly elliptic orbit between 1.2 AU at aphelion and 0.28 AU at perihelion. During the cruise phase, BepiColombo will cover the inner heliosphere between 1.2 and 0.3 AU and will perform some science observations (see details by Mangano et al. [this issue]). Even after the insertion of BepiColombo into Mercury orbit in December 2025, Mio will provide almost continuous in-situ measurements of the solar wind. Therefore, we will have a first chance to investigate the inner heliosphere with three points of measurement.

Here we focus on an overview of the Mio spacecraft, its operations, science operations plan, and science data handling and archiving. The overall BepiColombo mission overview is described by Benkhoff et al. [this issue] and the Mio-MPO coordinated observation plans are reported by Millilo et al. [this issue].

2. Spacecraft overview

Mio is an octagonal spin-stabilized satellite designed to measure in-situ plasma and electromagnetic fields from the orbit of Mercury. Figs. 1(a) and 1(b) show schematic drawings of Mio in its observational configuration. High-gain antenna (HGA) will be deployed before separation from MPO. After separation, medium-gain antenna (MGA) will be deployed and two pairs of electric field antenna and two extendable masts will be extended. Fig. 1(c) shows the flight model with both HGA and MGA deployed. The main structure of Mio consists of two panels (upper and lower), a central cylinder (thrust tube) and four bulkheads. Inside the central cylinder the batteries, nutation damper, and a tank for the cold N_2 gas jet system are located. A helical array antenna of 80 cm diameter excited by the radial line is adopted for the HGA system. The external appearance has an octagonal shape, which can be surrounded by a 1.8 m diameter circle. The height of the side panel is 1.1 m, with an upper portion covered up to 70% by solar cells and up to 30% by optical solar reflectors (OSRs). The lower portion is covered by OSRs and conductive white paint as seen in Fig. 1(c). The upper panel is located behind the boundary of the upper and lower portion of the side panel. Instruments are located on the upper and lower panels with an interval of 40 cm. The surface of the cover glass of solar cells and OSRs is coated by conductive material and connected to the spacecraft body in order to satisfy science requirements. The nominal spin period is 4-5 s (spin rate of ~15 rpm). The spin axis is pointed nearly perpendicular (92.5° [nominal] or 90° [alternative] depending on the orbital phase of the Mercury Revolution) to Mercury's orbital plane. Nominally Mio's spin axis will be controlled to satisfy the sun angle of 92.5° in order to prevent the shadow on the probe antennas due to the spacecraft body, which degrades the science return. During hot seasons near perihelion (true anomaly angle (TAA) < ±45°),

the spacecraft attitude will be changed to satisfy the sun angle of 90° in order to reduce solar heat inputs. Mio has four tangential thrusters on its side panels to control spin rate and two axial thrusters mounted at the bottom of the spacecraft to control the spin axis. These thrusters work only for attitude control and Mio thus does not have the capability to change its orbit. The spin axis direction is monitored by a star scanner located on the bottom of the spacecraft and spin rate is measured by a sun sensor on the side panel. The total mass of Mio at launch is 255 kg, including 3.7 kg N_2 gas for attitude and spin rate control. The total mass of the science payloads is 40 kg. The nominal mission of Mio is one Earth year and an extension of 1 year (or more) is expected. Technical point of view, the mission life will be determined by a lack of N_2 gas storage for attitude control or an impact of the spacecraft onto Mercury's surface because of gradually decreased periapsis altitude. Detailed specifications of Mio are given in Table 2.

Figure 2 shows the system block diagram of Mio. Special features of Mio's system design are as follows:

1. Unification of Data Handling Unit and Attitude Control Electronics into Data Management Controller (DMC).
2. The HGA can be pointed toward the Earth by the antenna despun motor (ADM), an elevation control mechanism, and the antenna pointing mechanism (APM).
3. Two types of MGA: one for command reception only (MGA) and another (MGA-TX) for data transmission using on-off keying. The beacon signal transmitted from MGA-TX is received on the ground for a short duration every one spin. MGA-TX transmits data by using on/off sequence of beacon signal modulation.
4. Power and telemetry/command interface to MPO for the cruise phase, since Mio does not generate power and both HGA and MGA are stowed. There are converters between MPO and Mio to adjust the bus voltage of MPO (28 V) to that of Mio (50 V). MIL-STD-1553B is used for command/telemetry data transmission between MPO and Mio. The bitrate for Mio telemetry data through MPO is 1 kB/s.
5. Thermal design to survive under Mercury's harsh environment. Figure 3 shows the concept of the thermal design of Mio. The basic concept of the thermal design is to minimize heat input from the environment and reject heat from the radiator. To realize this concept, the following design is used: a) side panels are thermally disconnected from the upper and lower panels by high-temperature conductive multilayer insulation (MLI); b) solar cells are mounted where the rear part of the side panel is exposed to space and covered by conductive OSRs to lower the temperature of the solar cell; c) lower parts of the side panels are covered by conductive OSRs or painted using conductive white paint; d) upper panel and HGA pedestal are covered by conductive high temperature MLI; e) HGA is painted by conductive white paint; and f) lower panel is covered by conductive OSRs and used as radiator.

6. There are two types of heater: a survival heater and an operational heater. The survival heater is regulated by a mechanical thermostat, whereas the operational heater is controlled by a software running on DMC according to the temperature sensor reading. Survival heaters are used when Mio is switched off (mainly in the cruise phase), and operational heaters are used when Mio is switched on (mainly after separation).

Mio carries five science instruments: Mercury Plasma Particle Experiment (MPPE), Magnetic Field Investigation (MGF), Plasma Wave Investigation (PWI), Mercury Sodium Atmosphere Spectral Imager (MSASI), and Mercury Dust Monitor (MDM). MPPE studies plasma and neutral particles from the planet, the magnetosphere, and interplanetary solar wind using seven sensors, i.e., Mercury Electron Analyzer (MEA1 and MEA2), Mercury Ion Analyzer (MIA), Mercury Mass Spectrum Analyzer (MSA), High-Energy Particle instrument for electron (HEP-ele), High-Energy Particle instrument for ion (HEP-ion), and Energetic Neutrals Analyzer (ENA) [Saito et al., 2010]. MEA1, MEA2, MIA, and MSA can cover 4π steradians using spacecraft spin. MGF studies the magnetic field of the planet, its magnetosphere, and interplanetary solar wind [Baumjohann et al., 2010]. MGF has two pairs of tri-axial flux magnetometers able to separate the natural magnetic field from the artificial field generated in the spacecraft. The inboard magnetometer (MGF-I) is mounted at the middle of a 5 m extendable mast for the magnetometer (MAST-MGF), and the outboard magnetometer (MGF-O) is mounted at the tip of MAST-MGF. PWI studies electric field, electromagnetic waves, and radio waves from the magnetosphere, as well as solar wind [Kasaba et al., 2010]. It uses two pairs of 15 m tip to root antenna (WPT and MEFISTO) to measure electric field. PWI also has a tri-axial search coil (SC) to measure the AC magnetic field. SC is mounted at the tip of 5 m extendable mast for SC (MAST-SC). MSASI studies the thin sodium exosphere of Mercury [Yoshikawa et al., 2010]. MDM studies dust, both from the planet and from interplanetary and interstellar space [Nogami et al., 2010]. Figure 4 shows the location of each sensor and a summary specification of all science instruments is given in Table 2. The Mio spacecraft coordinate system is also indicated in Figure 4. Figure 5 summarizes the field of view of each MPPE sensor. Details of each instrument are described in the papers of this issue [Kasaba et al., Saito et al., Kobayashi et al., Baumjohann et al., Murakami et al.]. Through combining data from MPPE, MGF, and PWI, full plasma parameters can be obtained with high time resolution. This reflects a significant improvement from MESSENGER, which did not carry wave instruments and for which the field of view of the particle instrument was limited. Hence many of the questions arising from MESSENGER observations are expected to be solved by Mio observations. The spin-stabilized spacecraft is, for example, the ideal platform for plasma measurements.

Mio has a highly elliptical polar orbit with initial periapsis and apoapsis heights of 590 and 11,649 km, respectively. The initial periapsis and apoapsis are close to the equatorial plane of Mercury and rotate slowly because of the gravitational coefficient. The relation of Mio's orbital plane and Mercury's orbit around the Sun is shown in Figure 6(a). The orbital plane of Mio is along the Sun-

Mercury line at perihelion (true anomaly angle (TAA) = 0°) and aphelion (TAA = 180°), and is perpendicular to the Sun-Mercury line at TAA = 90° or 270°. The apoapsis of Mio's orbit is at TAA = 0° for dayside and TAA = 180° at nightside. This orbit configuration was selected to relax the heat input from the hot surface of Mercury. Orbital configuration for TAA = 0°, 90°, and 180° are shown in Figures 6(b), 6(c), and 6(d), respectively. As shown in Figures 6(b) and 6(d), Mio has a long eclipse (maximum of 2 h) several days around TAA = 180° and short eclipse several days around TA = 0°. Mio stays in the upstream region of the solar wind most of the time and passes the nightside region close to the Mercury at TAA = 0° (Fig. 5(b)), therefore a small TAA would have been suitable to investigate upstream solar wind. While at TAA = 180° (Fig. 5(d)), Mio stays close to the magnetopause or in the magnetotail, giving a unique opportunity to investigate solar wind-magnetosphere interaction. As shown in Figure 6(c), Mio passes the duskside magnetosphere close to Mercury at TAA = 90°. Hence, Mio observes the magnetosphere close to Mercury as the planet revolves. Combining observations at TAA = 0° and 180° gives the distance dependence in the magnetosphere.

3. Operations overview

3.1 Mission scenario (phase definition)

Mio was launched on 20 October 2018 (Coordinated Universal Time, UTC) from the Guiana Space Center located in French Guiana by an Ariane 5 launcher. The Mercury Transfer Module (MTM), MPO, Mio and MMO sunshield and interface structure (MOSIF) are integrated together in the Mercury Composite Spacecraft (MCS) configuration, where Mio is positioned inside the MOSIF. Figure 7 shows the configuration of MCS for launch. Mio was not powered during launch, but survival heaters were activated as a part of the launch separation sequence.

Following the launch and early orbit phase, the mission moved to the near-Earth commissioning phase dedicated to the checkout of each spacecraft system, science instruments, and MCS performance evaluation. The first electrical propulsion arc started in December 2018, marking the beginning of the interplanetary cruise phase, which will last 7 years with nine planetary flybys in total.

The Mercury approach phase and Mio separation phase will be the most critical periods of activity for Mio throughout the whole mission. After MTM jettison, Mercury orbit insertion will start in December 2025. MPO thrusters will be used to bring the remaining composite spacecraft to Mio orbit, where Mio will be separated. MPO will then jettison the MOSIF and continue transitioning to its target orbit. Mio will execute critical post-separation operations autonomously, after which the two spacecrafts will start the Mercury orbit phase with a nominal duration of one Earth year.

3.2 Mode definition

The Mio operation mode in the MCS configuration is described below.

- Cruise Dormant: In this mode, only the survival heaters are powered by MPO to keep Mio

temperature within the non-operational range. Mio itself is off, therefore no telemetry is generated.
- Cruise Initial: This is the initial state after switching Mio power on. Most survival heaters are off in this mode, as the power is directed to Mio's components. Only DMC, Power Control and Distributer (PCD), X-band Transponder (XTRP-A/B) and converters are powered on. System Housekeeping (HK) telemetry is generated every second.
- Cruise Standby: In this mode, Mio operational heaters are activated and maintains the spacecraft in its operational temperature range. System HK telemetry is generated every 64 s, and command reception/execution is possible.
- Mio Cruise maintenance and checkout: This is the mode for conducting subsystem and science instrument checkout operations. Telemetry is generated every second and contains either System HK data or Mission HK/science data.

Transition between modes is performed using a dedicated Onboard Control Procedure (OBCP), which contains the necessary MPO and Mio command sequence and telemetry status checks. There is also a Mio emergency switch-off OBCP to quickly transfer to the dormant mode in case of major anomalies at MCS/MPO level.

3.3 Mission phase and Operation plan

The operations planned for each mission phase are explained below.

3.3.1 Near Earth commissioning phase

This phase was dedicated to initial checkout of the Mio spacecraft system and science instruments. In November 2018, Mio was brought into cruise maintenance and checkout mode for the first time after launch. The initial checkout was successfully completed by end of November 2018, and high-voltage checkout for the MPPE and MSASI instruments were conducted in June-August 2019. Launch lock release activities were also performed during this time. The checkout operations during this phase were mostly interactive, carried out at ESOC with real-time data transfer to the Sagamihara Space Operation Center (SSOC)/JAXA.

3.3.2 Interplanetary cruise phase

During the interplanetary cruise phase, operations are mainly executed by ESA ground stations [Montagnon et al., this issue]. Mio is kept in the dormant mode for the majority of the interplanetary cruise phase, except for the following activities:

(1) Cruise checkout

This is a periodic maintenance/checkout activity scheduled every 6-8 months. The main objective for Mio is a battery health check and, if required, charging. A functional check of all science instruments is also performed. These activities are executed using the MPO mission timeline and nominally

concludes within 1 day.

(2) Cruise science, flyby science observation

Mio is surrounded by MOSIF in cruise configuration, but some instruments have openings within their field of view and thus the opportunity for science observation during the cruise phase. Planetary flybys and interplanetary solar wind observations are under discussion. The observation sequence will be optimized based on trajectory prediction and the plasma region that the cruise composite will pass through. As a baseline plan, PWI (magnetic field), MGF, and MPPE- ENA/MSA/MIA/MEA/HEP-ele will be used for science measurements during planetary flybys.

(3) Maintenance/troubleshooting activities

Any other commissioning activities that are out of the scope of cruise checkout and science observation are discussed with the ESOC Flight Operations Team and implemented in the schedule as appropriate.

3.3.3 Mercury approach phase and separation

Mio will conduct the final system checks to prepare for separation, including charging the onboard battery, which is estimated to take 1 to 5 days depending on the charging current. After the MTM separation, the Marman clamp in Mio's spin ejection device will be released. The HGA is also deployed. The final separation tasks are executed by an OBCP, which will turn off the power to Mio (at this point, Mio is running on its own batteries), check the Mio separation readiness status, fire NEAs for harness separation, and finally fires the pyros to release Mio.

The Mio post-separation operation is initiated once mechanical separation is detected. All tasks are executed as onboard functions until a communication link to ground is established using the MGA/MGA-TX.

Once this link is made, interactive operations will proceed to confirm the spacecraft status and upload parameters for attitude control. The communication link will then be switched to HGA, and the extension sequences of MAST-SC, MAST-MGF and two pairs of wire antennas will be executed as follows: (1) Mio spin-up to 20 rpm, (2) sire antennas (MEFISTO-1, -2, WPT-1 and -2) deployment with 5 m steps, (3) MAST-SC and MAST-MGF deployment resulting in spin-down to ~9 rpm, and (4) spin-up to 15 rpm.

3.3.4 Mercury orbit phase

In this phase, the initial checkout of both the spacecraft bus system and science instruments are performed. For many instruments, this will be the first time in 7 years that full detailed functional checks are possible. The nominal operation of the Mio bus system can be categorized in routine operations. Daily tasks are the HGA pointing control and spin frequency control. Eclipse and Mercury occultation tables are updated every few days. Attitude (spin axis) control, battery reset operation, and

solar array panel UV level updates are each performed a certain number of times during each Mercury year (approximately 88 Earth days). There are also maintenance operations such as ACS timer reset, thrust parameter update, and heater control table updates, which will be performed as required.

The nominal science operations of Mio will be controlled at SSOC in JAXA/ISAS with communication from the Misasa Deep Space Station at Usuda Deep Space Center. The possibilities for future support by other ground stations are still under discussion. There are two kinds of operations plans: a long-term operations plan for one Mercury year and a short-term operations plan for one Earth week. The mission timeline will be updated with short-term planning twice per week.

4. Science operations plan at Mercury orbit phase

4.1 Baseline observation plan

Mio's main science target is Mercury's space environment, including solar wind and dust conditions. In order to maximize scientific outputs, continuous monitoring along the whole spacecraft orbit is important. Therefore, the baseline observation plan requests that all science instruments will be kept on, except for MSASI, a remote sensing instrument and the field of view will be directed downward from the bottom of the spacecraft such that its observation timing is limited from specific orbital positions [Yoshikawa et al., 2010; Murakami et al., this issue]. However, there are several major constraints for operations during Mercury orbit phase, and continuous measurements will not always be possible. Figure 8 shows Mercury's orbit and highlights periods of major constraints for Mio's science operations. One of the most critical constraints is temperature of the spacecraft and its instruments. Our thermal calculation for the Mercury orbit phase predicts that, during perihelion season, continuous operations of the payload will increase the temperature up to the unsustainable high values. To avoid this overheating, it is necessary to cease observations and turn off the science instruments during one to two orbits per three orbits, depending on TAA. We will update our thermal calculation using the latest thermal models and in-flight performances.

Another major constraint is electric power. Near aphelion the Mio spacecraft will experience a long eclipse with a duration of up to 120 min per orbit for ~7 Earth days. In order to keep the state of charge of the battery and to save its lifetime, science observations will be highly limited during this period. Battery charging requires about three times as long as the eclipse duration. Therefore, in the current baseline plan, no science observations are expected during this period. The aphelion season, however, is important from the scientific point of view, because Mio will normally be inside Mercury's magnetosphere and will cross the magnetotail region as shown in Figure 6d. The feasibility of science observations during an aphelion season will be carefully discussed and updated by checking the latest performance of battery, thermal characteristics, and electric power available and required for science instruments.

The science instruments have several observational modes that will be switched depending on the geometrical position of the spacecraft. For example, PWI and MPPE-MIA/MSA/MEA have a solar wind mode and magnetosphere mode. MPPE-ENA has three modes: periapsis mode, apoapsis mode, and a low-resolution mode for other regions. MSASI has a normal FOV mode (45° for spin scan) and wide FOV mode (90°). The timing of each mode change will be optimized at the initial phase of nominal operations, approximately one Mercury year after the start of science observations.

Nominal science operations will be performed by stored commands according to the onboard mission timeline. The number of commands for the mission timeline is limited to 512. The timeline will be updated twice per week, and one timeline sequence covers 1 week of operations for redundancy. Mio will have ~18 orbit revolutions per week, such that the upper limit for all instruments and spacecraft bus system will be about 28 commands per orbit on average. This limitation will not allow the observation modes to be changed many times during each orbit, and thus, careful observation planning is required. Some instruments requiring long observation sequences (e.g., MSASI) use long macro commands (the fixed sequence of commands stored in the onboard memory) to reduce the number of commands necessary.

4.2 Downlink strategy and baseline plan

Another important constraint on Mio's science observation is imposed by the downlink data rate from the spacecraft to the ground station, which varies strongly during the orbit phase. It is not possible to downlink all science data obtained by the payloads; rather, it is a necessary need to select a part of them. In order to maximize science output against such a limitation of downlink data size, we have three data modes with different resolutions and downlink priorities: low-resolution (L-) mode for continuous monitoring and event survey, nominal (M-) mode for standard science analysis, and burst (H-) mode for high-quality analysis. All scientific instruments generate L-mode data, all of which will be downlinked in quasi-real time (within 1 day). M-mode data are generated at the same time (except for MDM, MPPE-ENA, PWI-AM2P, and MSASI) and can be stored in the spacecraft data recorder for ~9 days. Because of the constraint on a downlink data rate, only 20%-30% of the M-mode data can be downlinked. Thus, the strategy to mitigate this constraint is to downlink L-mode data first and then select M-mode data to be downlinked by checking the L-mode data quick-looks. The plasma measurement suite (MGF, PWI, and MPPE) has the H-mode based on 4-20 min interval data sets. The H-mode data is taken by a preset mission timeline or by onboard automatic triggering. In order to optimize the parameters and thresholds for automatic trigger detection, we need to investigate data for at least one Mercury year during the Mercury orbit phase. All science data processing is performed by the Mission Data Processor (MDP) [Kasaba et al., this issue].

Based on the assumptions shown in Table 4, the downlink data rate for the Mercury orbit phase can be estimated. The average downlink rate for science data is 3.7 kbps (38 MB/day). Figure 9 shows the

result of our data rate calculation. The thick black line shows the total data size that can be downlinked each day. The daily-averaged downlink rate depends on the distance between Earth and Mercury, Mercury occultation, and thermal and electric power constraints for spacecraft communication. The red and blue lines in Figure 9 show the data production rate of L-mode and L- and M-mode, respectively. Figure 9 clearly indicates that all L-mode data can be downlinked but M-mode data require a selective downlink. The original design of the downlink plan for each data mode is described by Kasaba et al. [this issue].

As shown in Figure 9, the downlink data rate is highly variable in time. For example, during Mercury year (MY) #1 and #2, we can downlink a huge volume of data, but on the other hand we will have very low downlink rates in MY #3 and #4. Table 5 shows the summary of averaged downlink data rates for each observation period. It is necessary to establish an optimized plan to downlink science data effectively for each period. In order to deal with this strategy, we have two kinds of operations plan: a long-term operations plan with a duration of one Mercury year and a short-term plan for 1-week operations, planned to be uploaded twice a week.

We need to decide which M-mode (and H-mode) data should be downlinked as early as possible, because the onboard data recorder can store only ~9 days' data. In order to achieve this selective downlink quickly and effectively, we have a strategy of downlink request with several priorities as follows. We prepare a baseline long-term plan for downlink every Mercury year, on the basis of the spacecraft position along the orbit and expected downlink rate. A few days after the observation, additional downlink requests with higher priority will come from event detection by the L-mode data survey if that period is not covered in the baseline plan. In addition, if any Mio-MPO-coordinated observations are planned, the data resulting from this period has the highest priority for downlink.

In order to prepare a baseline downlink plan, the spacecraft position is most important, especially relative to Mercury's magnetosphere. The duration of the period when Mio is inside the magnetosphere is shown in Figure 10. We used the KT17 model [Korth et al., 2017] with a disturbance index of 50% for calculating the location of the magnetopause. As shown in Figure 10, Mio stays within the solar wind most of the time and inside the magnetosphere just ~11% of the time, except for during near aphelion season (TAA = 180°). Thus, we can downlink most M-mode data obtained inside the magnetosphere. During periods of high downlink rate such as MY #1 and #2, we can add the solar wind M-mode and H-mode data to the selective downlink requests. On the other hand, when a very low downlink data rate exists, as in MY #4, specific parts of magnetospheric M-mode data must be selected. Downlink strategies will be prepared in more detail after the thermal analysis update.

5. Data handling and archiving

5.1 Data pipeline and archiving plan

Figure 11 shows the outline of the science data pipeline. Science data obtained by Mio is

automatically stored into the scientific information retrieval and integrated utilization system (SIRIUS), the telemetry database of JAXA [Nomura et al. 1983]. All telemetry data from Mio are compliant with the CCSDS-binary format. Instrument teams retrieve the raw CCSDS-binary data (Level-0 data) from SIRIUS and process these data to make Level-1 data. Level-1 data carry time labels in UTC, whereas observed data are uncalibrated (instrument-dependent units.) Level-1 data are converted to Level-1p (calibrated) data in standard physical units by the instrument teams. ISAS converts Level-1p data to official public-open version data (Level-2 data). The adequate metadata (e.g., rules of the road) are attached to the Level-2 data. Level-2 data are in accordance with the PDS4 convertible format (see Section 5.2 for data formatting). Level-2 data are made available to users on a dedicated server soon after data processing and are archived in the data archives and transmission system (DARTS) for long-term archiving. All generated Level-2 data are converted to the PDS4 format for planetary research users. The converted Level-2 PDS4 data are archived in DARTS. Level-3 data reflect the combined products of multiple Level-2 data from different instruments (e.g., pitch angle distributions of particle fluxes.) The basic idea of data level definition is based on the Arase case [Miyoshi et al. 2018a, 2018b]. A summary of the definition of the science data level is shown in Table 6.

We perform time labeling in UTC when we generate Level-1 data. A time index (TI), which is a time-sequential counter (LSB = 31.25 ms) using the internal clock of the spacecraft bus-system, is attached to every data packet from Mio. A corresponding UTC can be calculated from attached TI using a time-calibration table. An MDP-TI (LSB = 1.95 ms) is also attached to every mission packet to determine the time label.

Raw CCSDS binary data (Level-0 data) nominally become available within 1-2 working days after receiving telemetry data from Mio. The daily tasks of Level-1, Level-1p, Level-2, and Level-3 data generation are automatically processed on the workstation after Level-0 data become available on SIRIUS. Processed Level-2 data will be publicly available on both the dedicated server and DARTS according to a project-agreed schedule.

We provide orbit, attitude, and other ancillary data as a SPICE kernel. SPICE is developed by the Navigation and Ancillary Information Facility team of the Jet Propulsion Laboratory (NASA) and widely used to determine observation geometry for planning and analyzing space science observations.

5.2 Data format

We adopt the common data format (CDF) as the standard format of Level-2 science data products. CDF is proposed by the National Space Science Data Center/NASA and is commonly used for archiving solar-terrestrial physics data (e.g., Arase (Miyoshi et al. 2018a), Van Allen probes (Mauk et al. 2012), MMS (Burch et al. 2016), and many other solar-terrestrial physics missions). In the case of Arase, all of science data (plasma wave data and plasma particle data) are archived in CDF and

distributed by the ERG Science center (Miyoshi et al. 2018b). Because the basic design of plasma particle and wave instruments aboard Mio is almost the same as that of Arase, a part of the existing tools and technique can be used for Mio data processing and archiving.

On the other hand, there are cases in which CDF is not suitable when we archive image-like data. For archiving imaging observation data, the flexible image transport system (FITS) is widely used (e.g., Hisaki mission; Yoshikawa et al. 2014). Therefore, we have adopted the FITS format for data obtained by MSASI. Regarding the MDM data, we provide Level-2 data in the ASCII format because they have a relatively simple list of dust detections.

All Level-2 CDF/FITS/ASCII data are converted into PDS4 format for users in the field of planetary research. The contents of Level-2 PDS4 data are the same as those of Level-2 CDF/FITS/ASCII data.

5.3 Data analysis tools

All Level-2 CDF/FITS/ASCII data can be analyzed by the Space Physics Environment Data Analysis Software (SPEDAS) (Angelopoulos et al. 2018). SPEDAS is a suite of scientific analysis routines written in Interactive Data Language (IDL), and widely used in solar-terrestrial physics. Users can easily download Level-2 data via the internet using the load procedure and create combined plots using multiple data products. The SPEDAS will be also used for the generation of quick-look plots.

6. Conclusions

The BepiColombo mission will provide the first comprehensive investigation of Mercury with two spacecraft. The Mio spacecraft is designed to analyze Mercury's environment, one of the most unique and complex systems in the Solar System featuring a range of interactions between the intense solar wind, planetary surface, weak global magnetic field, tenuous exosphere, and dynamic magnetosphere. The main science targets of Mio are (1) to assess the structure and origin of Mercury's magnetic field; (2) to analyze the structure, dynamics, and physical processes in Mercury's magnetosphere; (3) to study the structure, variation, and origin of Mercury's exosphere; and (4) to determine the physical environment of the inner heliosphere. Mio will address unsolved questions on these targets raised by MESSENGER with new investigations focusing on plasma waves, energetic neutral atoms, low-energy electrons, and dust monitoring, and with higher instrumental capabilities such as wider energy ranges of plasma particles and a higher resolution of spectral imaging in the exosphere. The spin-stabilized platform also significantly enhances the capability of plasma particle measurements relative to other three-axis stabilized spacecraft.

After the launch of BepiColombo on 20 October 2018, initial checkout operations of the Mio spacecraft system and science instruments were successfully performed. During the 7 years cruise phase, periodic maintenance/checkout activities of the spacecraft bus system (mainly the battery) and instruments are planned to take place every 6-8 months. Though the capabilities of the science

instruments are limited during the cruise phase because of the stacked spacecraft configuration and unextended wire antennas and masts, we plan science observations for planetary flybys at the Earth, Venus, and Mercury. Solar wind measurements during the cruise can also contribute to inner-heliospheric science in coordination with other spacecraft such as NASA's Parker Solar Probe and ESA's Solar Orbiter and ground-based observations. After the Mercury orbit insertion, most critical operations such as spacecraft separation and the extension of wire antennas and masts will be executed.

Nominal science operations during the Mercury orbit phase are strongly constrained by the thermal condition during the aphelion season and electric power during the long eclipse period in the perihelion season. The baseline observation plan of Mio will conduct continuous measurements as long as possible against the major constraints above (except for MSASI). The downlink plan is more complicated and requires optimization. On the basis of the highly variable expected downlink data rate due to the distance between the Earth and Mercury, we have prepared the downlink strategy for each Mercury year. All low-resolution (L-mode) data and 20%-30% of nominal resolution (M-mode) data will be downlinked. The downlink plan plays a key role in maximizing the science outputs of Mio, and we will continue to discuss and update it within the science working group. Science data will be processed based on heritages from the past missions and high-level products will be prepared in both CDF/FITS/ASCII format and PDS4 format.

Acknowledgments

The authors wish to express sincere appreciation to all the members in the PI teams, the Mio science working group, the project teams of JAXA and ESA, and the industries for their long contributions to science managements, spacecraft developments, testing, and operations planning. Especially the authors would like to thank Dr. Hiroshi Yamakawa, Dr. Toshifumi Mukai, Dr. Hiroshi Matsumoto, Dr. Jean-Louis Bougeret, Dr. Lars Blomberg, Dr. Ken'ichi Nogami, Dr. Hiromi Shibata, and Dr. Jean-Andre Sauvaud for their efforts to the mission from the beginning.

References

Angelopoulos, V., P. Cruce, A. Drozdov. E. W. Grimes. N. Hatzigeorgiu, D. A. King, D. Larson, J. W. Lewis, J. M. McTiernan, D. A. Roberts, C. L. Russell, T. Hori, Y. Kasahara, A. Kumamoto, A. Matsuoka, Y. Miyashita, Y. Miyoshi, I. Shinohara, M. Teramoto, J. B. Faden, A. J. Halford, M. McCarthy, R. M. Millan, J. G. Sample, D. M. Smith, L. A. Woodger, A. Masson, A. A. Narock, K. Asamura, T. F. Chang, C.-Y. Chiang, Y. Kazama, K. Keika, S. Matsuda, T. Segawa, K. Seki, M. Shoji, S. W. Y. Tam, N. Umemura, B.-J. Wang, S.-Y. Wang, R. Redmon, J. V. Rodriguez, H. J. Singer, J. Vandegriff, S. Abe, M. Nose, A. Shinbori, Y.-M. Tanaka, S. UeNo, L. Andersson, P. Dunn, C. Fowler, J. S. Halekas, T. Hara, Y. Harada, C. O. Lee, R. Lillis, D. L. Mitchell, M. R. Argall, K. Bromund, J. L. Burch, I. J. Cohen, M. Galloy, B. Giles, A. N. Jaynes, O. Le Contel, M. Oka, T. D. Phan, B. M.

541 Walsh, J. Westlake, F. D. Wilder, S. D. Bale, R. Livi, M. Pulupa, P. Whittlesey, A. DeWolfe, B. Harter,
542 E. Lucas, U. Auster, J. W. Bonnell, C. M. Cully, E. Donovan, R. E. Ergun, H. U. Frey, B. Jackel, A.
543 Keiling, H. Korth, J. P. McFadden, Y. Nishimura, F. Plaschke, P. Robert, D. L. Turner, J. M. Weygand,
544 R. M. Candey, R. C. Johnson, T. Kovalick, M. H. Liu, R. E. McGuire, A. Breneman, K. Kersten, P.
545 Schroeder, The Space Physics Environment Data Analysis System (SPEDAS), Space Sci. Rev., 215:
546 9, doi:10.1007/s11214-018-0576-4, 2019.
547 Baumjohann, Wolfgang; Matsuoka, Ayako; Magnes, Werner; Glassmeier, Karl-Heinz; Nakamura,
548 Rumi; Biernat, Helfried; Delva, Magda; Schwingenschuh, Konrad; Zhang, Tielong; Auster, Hans-
549 Ulrich; Fornacon, Karl-Heinz; Richter, Ingo; Balogh, André; Cargill, Peter; Carr, Chris; Dougherty,
550 Michele; Horbury, Timothy S.; Lucek, Elizabeth A.; Tohyama, Fumio; Takahashi, Takao Tanaka,
551 Makoto; Nagai, Tsugunobu; Tsunakawa, Hideo; Matsushima, Masaki; Kawano, Hideaki; Yoshikawa,
552 Akimasa; Shibuya, Hidetoshi; Nakagawa, Tomoko; Hoshino, Masahiro; Tanaka, Yoshimasa;
553 Kataoka, Ryuho; Anderson, Brian J.; Russell, Christopher T.; Motschmann, Uwe; Shinohara, Manabu,
554 Magnetic field investigation of Mercury's magnetosphere and the inner heliosphere by MMO/MGF,
555 Planetary Space Sci., Volume 58, Issue 1-2, p. 279-286, doi:10.1016/j.pss.2008.05.019, 2010.
556 Baumjohann, W., A. Matsuoka, Y. Narita, W. Magnes, D.Heyner, K.-H. Glassmeier, R. Nakamura, D.
557 Fischer, F. Plaschke, M. Volwerk, T. L. Zhang, H.-U. Auster, I. Richter, A. Balogh, C. Carr, M.
558 Dougherty, T. S. Horbury, H. Tsunakawa, M. Matsushima, M. Shinohara, H. Shibuya, T. Nakagawa,
559 M. Hoshino, Y. Tanaka, B. J. Anderson, C. T. Russell, U. Motschmann, F. Takahashi, and A. Fujimoto,
560 The BepiColombo-Mio Magnetometer en Route to Mercury, Space Sci. Rev., this issue.
561 Benkhoff, Johannes; van Casteren, Jan; Hayakawa, Hajime; Fujimoto, Masaki; Laakso, Harri; Novara,
562 Mauro; Ferri, Paolo; Middleton, Helen R.; Ziethe, Ruth, BepiColombo—Comprehensive exploration
563 of Mercury: Mission overview and science goals, Planetary Space Sci., Volume 58, Issue 1-2, p. 2-
564 20, doi:10.1016/j.pss.2009.09.020, 2010.
565 Benkhoff, J., S. Besse, H. Hayakawa, G. Murakami, M. Novara, U. Reininghaus, D. Stramaccioni, O.
566 Sutherland, J. Zender, and the BepiColombo team, BepiColombo - mission overview and science
567 goals, Space Sci. Rev., this issue.
568 Burch, J. L., T. E. Moore, R. B. Torbert, B. L. Giles, Magnetospheric Multiscale Overview and Science
569 Objectives, Space Sci. Rev., 199, 1, pp 5–21, doi: 10.1007/s11214-015-0164-9, 2016.
570 Cassidy, T. A., A. W. Merkel, M. H. Burger, W. E. McClintock, R. M. Killen, M. Sarantos, A. L.
571 Sprague, R. J. Vervack, Jr., S. C. Solomon, Mercury’s Seasonal Sodium Exosphere: MESSENGER
572 Orbital Observations, Icarus, 248, 547-559, doi:10.1016/j.icarus.2014.10.037, 2015.
573 Dewey, R. M., J. M. Raines, W. Sun, J. A. Slavin, and G. Poh, MESSENGER Observations of Fast
574 Plasma Flows in Mercury's Magnetotail, Geophys. Res. Lett., 45, 10,110-10,118, doi:
575 10.1029/2018GL079056, 2018.
576 Dong, C., M. Lingam, Y. J. Ma, and O. Cohen, Is Proxima Centauri B habitable? A study of

577 atmospheric loss, ApJ Letters, 837, L26, 2017.
578 Dong, C., M. Jin, M. Lingam, V. S. Airapetian, Y. J. Ma, B. van der Holst, Atmospheric escape from
579 the TRAPPIST-1 planets and implications for habitability, Proceedings of the National Academy of
580 Sciences, 115, 260-265, doi:10.1073/pnas.1708010115, 2018.
581 Fox, N. J., M. C. Velli, S. D. Bale, R. Decker, A. Driesman, R. A. Howard, J. C. Kasper, J. Kinnison,
582 M. Kusterer, D. Lario, M. K. Lockwood, D. J. McComas, N. E. Raouafi, and A. Szabo, The Solar
583 Probe Plus Mission: Humanity's First Visit to Our Star, Space Sci. Rev., Volume 204, Issue 1-4, pp.
584 7-48, doi:10.1007/s11214-015-0211-6, 2016.
585 Gillon, M., A. H. M. J. Triaud, B.-O. Demory, E. Jehin, E. Agol, K. M. Deck, S. M. Lederer, J. de Wit,
586 A. Burdanov, J. G. Ingalls, E. Bolmont, J. Leconte, S. N. Raymond, F. Selsis, M. Turbet, K. Barkaoui,
587 A. Burgasser, M. R. Burleigh, S. J. Carey, A. C. C. M. Chaushev, L. Delrez, C. S. Fernandes, D. L.
588 Holdsworth, E. J. Kotze, V. Van Grootel, Y. Almleaky, Z. Benkhaldoun, P. Magain, and D. Queloz,
589 Seven temperate terrestrial planets around the nearby ultracool dwarf star TRAPPIST-1, Nature,
590 Volume 542, Issue 7642, pp. 456-460, doi:10.1038/nature21360, 2017.
591 Hayakawa, H., Y. Kasaba, H. Yamakawa, H. Ogawa, and T. Mukai, The BepiColombo/MMO model
592 payload and operation plan, Advances in Space Research, Volume 33, Issue 12, p. 2142-2146,
593 doi:10.1016/S0273-1177(03)00438-1, 2004.
594 Kasaba, Y., J. -L. Bougeret, L. G. Blomberg, H. Kojima, S. Yagitani, M. Moncuquet, J. -G. Trotignon,
595 G. Chanteur, A. Kumamoto, Y. Kasahara, J. Lichtenberger, Y. Omura, K. Ishisaka, and H. Matsumoto,
596 The Plasma Wave Investigation (PWI) onboard the BepiColombo/MMO: First measurement of
597 electric fields, electromagnetic waves, and radio waves around Mercury, Planetary Space Sci.,
598 Volume 58, Issue 1-2, p. 238-278, doi:10.1016/j.pss.2008.07.017, 2010.
599 Kasaba, Y., H. Kojima, M. Moncuquet, J.-E. Wahlund, S. Yagitani, F. Sahraoui, P. Henri, T. Karlsson,
600 Y. Kasahara, A. Kumamoto, K. Ishisaka, K. Issautier, G. Wattieaux, T. Imachi, S. Matsuda, J.
601 Lichtenberger, and H. Usui, Plasma Wave Investigation (PWI) aboard BepiColombo Mio on the trip
602 to the first measurement of electric fields, electromagnetic waves, and radio waves around Mercury,
603 Space Sci. Rev., this issue.
604 Kasaba, Y., T. Takashima, S. Matsuda, S. Eguchi, M. Endo, T. Miyabara, M. Taeda, Y. Kuroda, Y.
605 Kasahara, T. Imachi, H. Kojima, S. Yagitani, M. Moncuquet, J.-E. Wahlund, A. Kumamoto, A.
606 Matsuoka, W. Baumjohann, S. Yokota, K. Asamura, Y. Saito, D. Delcourt, M. Hirahara, S. Barabash,
607 N. Andre, M. Kobayashi, I. Yoshikawa, G. Murakami, and H. Hayakawa, Mission Data Processor
608 aboard the BepiColombo Mio Spacecraft: Design and Scientific Operation Concept, Space Sci.
609 Rev.,216, article id.34, doi:10.1007/s11214-020-00658-x, 2020.
610 Kobayashi, M. H. Shibata, K. Nogami, M. Fujii, T. Hirai, S. Hasegawa, M. Hirabayashi, T. Iwai, H.
611 Kimura, T. Miyachi, M. Nakamura, H. Ohashi, S. Sasaki, S. Takechi, H. Yano, S. R. Srama, H. Krüger,
612 P. Strub, A.-K. Lohse, E. Grün, Mercury Dust Monitor (MDM) onboard the Mio orbiter of the

613 BepiColombo mission, Space Sci. Rev., this issue.
614 Korth, H., C. L. Johnson, L. Philpott, N. A. Tsyganenko, and B. J. Anderson, A Dynamic Model of
615 Mercury's Magnetospheric Magnetic Field, Geophys. Res. Lett., Volume 44, Issue 20, pp. 10,147-
616 10,154, doi:10.1002/2017GL074699, 2017.
617 Lawrence, D. J., B. J. Anderson, D. N. Baker, W. C. Feldman, G. C. Ho, H. Korth, R. L. McNutt, P. N.
618 Peplowski, S. C. Solomon, R. D. Starr, J. D. Vandegriff, and R. M. Winslow, Comprehensive survey
619 of energetic electron events in Mercury's magnetosphere with data from the MESSENGER Gamma-
620 Ray and Neutron Spectrometer, J. Geophys. Res., 120, 2851-2876, doi:10.1002/2014JA020792, 2015.
621 Lindsay, S.T., M. K. James, E. J. Bunce, S. M. Imber, H. Korth, A. Martindale, and T. K. Yeoman,
622 MESSENGER X-ray observations of magnetosphere-surface interaction on the nightside of Mercury.
623 Planetary Space Sci. 125, 72-79, doi:10.1016/j.pss.2016.03.005, 2016.
624 Mangano, V., et al., BepiColombo science investigations during cruise and during flybys at the Earth,
625 Venus and Mercury, Space Sci. Rev., this issue.
626 Mauk, B. H., N. J. Fox, S. G. Kanekal, R. L. Kessel, D. G. Sibeck, A. Ukhorskiy, Science Objectives
627 and Rationale for the Radiation Belt Storm Probes Mission, Space Sci. Rev., 179, 1, pp 3–27,
628 doi:10.1007/s11214-012-9908-y, 2013.
629 McClintock, W. E., R. J. Vervack, Jr., E. T. Bradley, R. M. Killen, A. L. Sprague, and N. R. Izenberg,
630 Mercury’s Exosphere: Observations MESSENGER’s First Mercury Flyby, Science, 321, 92-94, 2008.
631 McClintock, W. E., R. J. Vervack, Jr., E. T. Bradley, R. M. Killen, N. Mouawad, A. L. Sprague, M. H.
632 Burger, S. C. Solomon, and N. R. Izenberg, Mercury's Exosphereduring MESSENGER’s Second
633 Flyby: Detection of Magnesium and Distinct Distributions of Neutral Species, Science, 324, 610-
634 613, 2009.
635 Milillo, A., P. Wurz, S. Orsini, D. Delcourt, E. Kallio, R. M. Killen, H. Lammer, S. Massetti, A. Mura,
636 S. Barabash, G. Cremonese, I. A. Daglis, E. Angelis, A. M. Lellis, S. Livi, V. Mangano, and K. Torkar,
637 Surface-Exosphere-Magnetosphere System Of Mercury, Space Sci. Rev., Volume 117, Issue 3-4, pp.
638 397-443, doi:10.1007/s11214-005-3593-z, 2005.
639 Milillo, A., M. Fujimoto, G. Murakami, J. Benkhoff, J. Zender, S. Aizawa, M. Dósa, L. Griton, D.
640 Heyner, G. Ho, S.M. Imber, X. Jia, T. Karlsson, R.M. Killen, M. Laurenza, S.T. Lindsay, S.
641 McKenna-Lawlor, A. Mura, J.M. Raines, D.A. Rothery, N. André, W. Baumjohann, A. Berezhnoy,
642 P.A. Bourdin, E.J. Bunce, F. Califano, J. Deca, S. de la Fuente, C. Dong, C. Grava, S. Fatemi, P.
643 Henri, S.L. Ivanovski, B. V. Jackson, M. James, E. Kallio, Y. Kasaba, E. Kilpua, M. Kobayashi, B.
644 Langlais, F. Leblanc, C. Lhotka, V. Mangano, A. Martindale, S. Massetti, A. Masters, M. Morooka,
645 Y. Narita, J.S. Oliveira, D. Odstrcil, S. Orsini, M.G. Pelizzo, C. Plainaki, F. Plaschke, F. Sahraoui, K.
646 Seki, J.A. Slavin, R. Vainio, P. Wurz, S. Barabash, C.M. Carr, D. Delcourt, K.-H. Glassmeier, M.N.
647 Grande, M. Hirahara, J. Huovelin, O. Korablev, H. Kojima, H. Lichtenegger, S. Livi, A. Matsuoka,
648 R. Moissl, M. Moncuquet, K. Muinonen, E. Quèmerais, Y. Saito, S. Yagitani, I. Yoshikawa, and J.-E.

649 Wahlund, Investigating Mercury's environment with the two-spacecraft BepiColombo mission,
650 Space Sci. Rev., this issue.
651 Miyoshi, Y., I. Shinohara, T. Takashima, K. Asamura, N. Higashio, T. Mitani, S. Kasahara, S. Yokota,
652 Y. Kazama, S-Y. Wang, P. Ho, Y. Kasahara, Y. Kasaba, S. Yagitani, A. Matsuoka, H. Kojima, Y. Katoh,
653 K. Shiokawa, K. Seki, Geospace exploration project ERG, Earth Planets Space, 70, 101,
654 doi:10.1186/s40623-018-0862-0, 2018a.
655 Miyoshi, Y., Hori, T., Shoji, M., M. Teramoto, T. F. Chang, T. Segawa, N. Umemura, S. Matsuda, S.
656 Kurita, K. Keika, Y. Miyashita, K. Seki, Y. Tanaka, N. Nishitani, S. Kasahara, S. Yokota, A. Matsuoka,
657 Y. Kasahara, K. Asamura, T. Takashima, I. Shinohara, The ERG Science Center, Earth Planets Space,
658 70, 96, doi:10.1186/s40623-018-0867-8, 2018b.
659 Montagnon, E., C. Steiger, F. Budnik, T.Seki, G. Murakami, M. Ogawa, M.Yamashita, and M. Casale,
660 BepiColombo Ground Segment and Mission Operations, Space Sci. Rev., this issue.
661 Müller, D., R. G. Marsden, O. C. St. Cyr, and H. R. Gilbert, Solar Orbiter-Exploring the Sun-
662 Heliosphere Connection, Solar Physics, Volume 285, Issue 1-2, pp. 25-70, doi:10.1007/s11207-012-
663 0085-7, 2013.
664 Mura, A., P. Wurz, J. Schneider, H. Lammer, J.-M. Grießmeier, M.L. Khodachenko, J. Weingrill, E.
665 Guenther, J. Cabrera, A. Erikson, M. Fridlund, A. Milillo, H. Rauer, Ph. von Paris, Comet-like Na
666 and Ca exospheres of hot rocky exoplanets: possible implications for Corot-7b, Icarus, 211, 1, 1-9
667 doi:10.1016/j.icarus.2010.08.015, 2011.
668 Murakami, G., I. Yoshikawa, S. Kameda, O. Korablev, V. Kottsov, M. Kuwabara, T. Sato, Y. Suzuki,
669 K. Yoshioka, and A. Tavrov, Mercury Sodium Atmosphere Spectral Imager (MSASI) onboard the
670 BepiColombo/Mio spacecraft: overviews, calibrated performances, and observation plans, Space Sci.
671 Rev., this issue.
672 Nogami, K., M. Fujii, H. Ohashi, T. Miyachi, S. Sasaki, S. Hasegawa, H. Yano, H. Shibata, T. Iwai, S.
673 Minami, S. Takechi, E. Grün, and R. Srama, Development of the Mercury dust monitor (MDM)
674 onboard the BepiColombo mission, Planetary Space Sci., Volume 58, Issue 1-2, p. 108-115,
675 doi:10.1016/j.pss.2008.08.016, 2010.
676 Nomura, T., Y. Sekiguchi, and T. Kato, On the scientific information retrieval and integrated utilization
677 system. In: Proceedings of symposium on scientific satellites, institute of space and astronautical
678 science, pp 37–40, 1983.
679 Saito, Y., J. A. Sauvaud, M. Hirahara, S. Barabash, D. Delcourt, T. Takashima, K. Asamura, and
680 BepiColombo MMO/MPPE Team, Scientific objectives and instrumentation of Mercury Plasma
681 Particle Experiment (MPPE) onboard MMO, Planetary Space Sci., Volume 58, Issue 1-2, p. 182-200,
682 doi:10.1016/j.pss.2008.06.003, 2010.
683 Saito, Y., D. Delcourt, M. Hirahara, S. Barabash, N. Andre, T. Takashima , K. Asamura, S. Yokota,
684 M.N. Nishino, J.-A. Sauvaud, C. Aoustin, A. Barthe, A. Cadu, A. Fedorov, A.-M. Frezoul, C. Garat,

E. Le Comte, Q.-M. Lee, J.-L. Medale, D. Moirin, E. Penou, M. Petiot, G. Peyre, J. Rouzaud, H.-C. Seran, W. Miyake, I. Shinohara, H. Hasegawa, K. Seki, A. Coates, F. Leblanc, C. Verdeil, B. Katra, D. Fontaine, J.-M. Illiano, J.-J. Berthelier, M. Fraenz, H. Fischer, N. Krupp, H. Krueger, B. Fiethe, H. Michalik, T. Mitani, W.-H. Ip, M. Hoshino, M. Fujimoto, N.Terada, Y. Harada, K. Keika, Pre-flight calibration and near-earth commissioning results of Mercury Plasma Particle Experiment (MPPE) onboard MMO (Mio), Space Sci. Rev., this issue.

Slavin, J. A., B. J. Anderson, D. N. Baker, M. Benna, S. A. Boardsen, G. Gloeckler, R. E. Gold, G. C. Ho, H. Korth, S. M. Krimigis, R. L. McNutt, L. R. Nittler, J. M. Raines, M. Sarantos, D. Schriver, S. C. Solomon, R. D. Starr, P. M. Trávníček, M. Pavel, and T. H. Zurbuchen, MESSENGER observations of extreme loading and unloading of Mercury's magnetic tail, Science, 329(5992), 665–668, doi:10.1126/science.1188067, 2010.

Solomon, S. C., R. L. McNutt, R. E. Gold, and D. L. Domingue, MESSENGER Mission Overview, Space Sci. Rev., Volume 131, Issue 1-4, pp. 3-39, doi:10.1007/s11214-007-9247-6, 2007.

Yamakawa, H., H. Ogawa, Y. Sone, H. Hayakawa, Y. Kasaba, T. Takashima, T. Mukai, T. Tanaka, and M. Adachi, BepiColombo Mercury magnetospheric orbiter design, Acta Astronautica, 62,699–705, doi:10.1016/j.actaastro.2008.01.040, 2008.

Yoshikawa, I., O. Korablev, S. Kameda, D. Rees, H. Nozawa, S. Okano, V. Gnedykh, V. Kottsov, K. Yoshioka, G. Murakami, F. Ezawa, and G. Cremonese, The Mercury sodium atmospheric spectral imager for the MMO spacecraft of Bepi-Colombo, Planetary Space Sci., Volume 58, Issue 1-2, p. 224-237, doi:10.1016/j.pss.2008.07.008, 2010.

Yoshikawa, I., K. Yoshioka, G. Murakami, A. Yamazaki, F. Tsuchiya, M. Kagitani, T. Sakanoi, N. Terada, T. Kimura, M. Kuwabara, K. Fujiwara, T. Hamaguchi, H. Tadokoro (2014), Extreme Ultraviolet Radiation Measurement for Planetary Atmospheres/Magnetospheres from the Earth-Orbiting Spacecraft (Extreme Ultraviolet Spectroscope for Exospheric Dynamics: EXCEED), Space Sci. Rev., 184, 1, pp 237–258, doi: 10.1007/s11214-014-0077-z

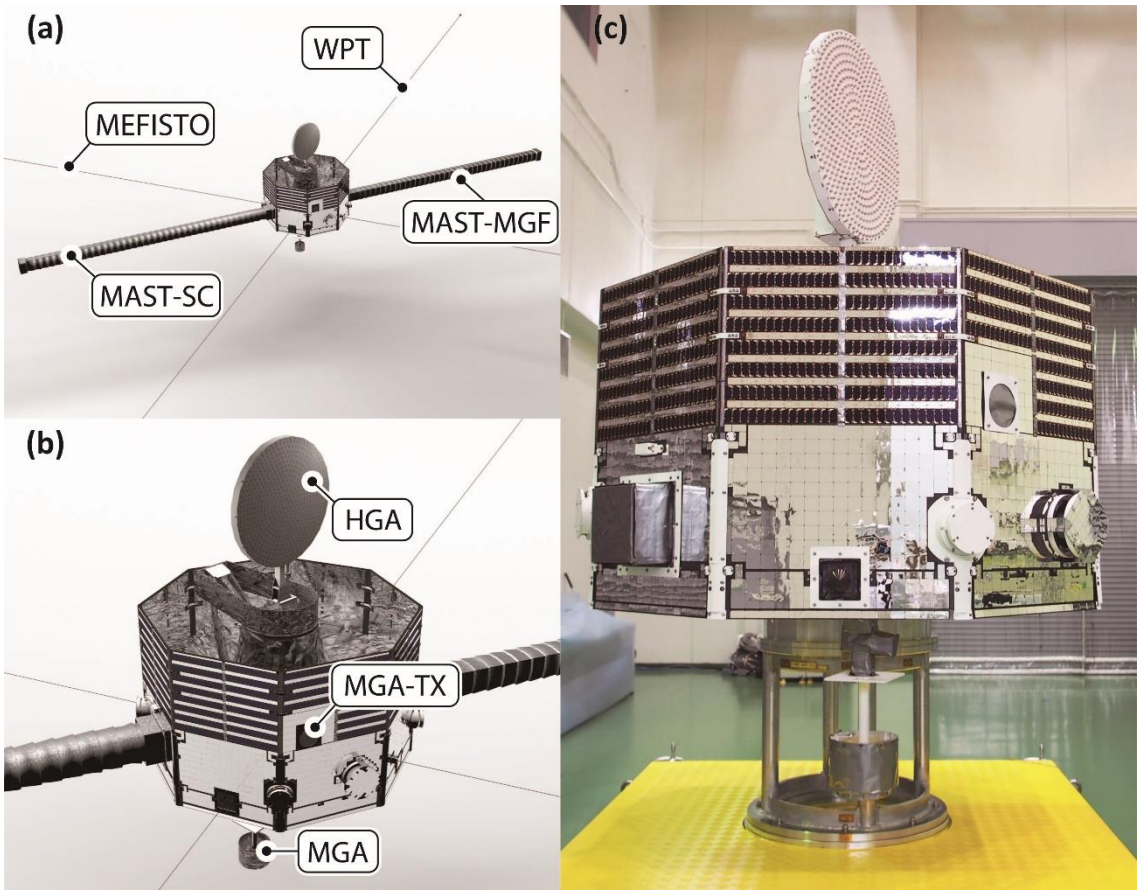

Figure 1: Schematic views (a, b) and photograph (c) of the Mio spacecraft.

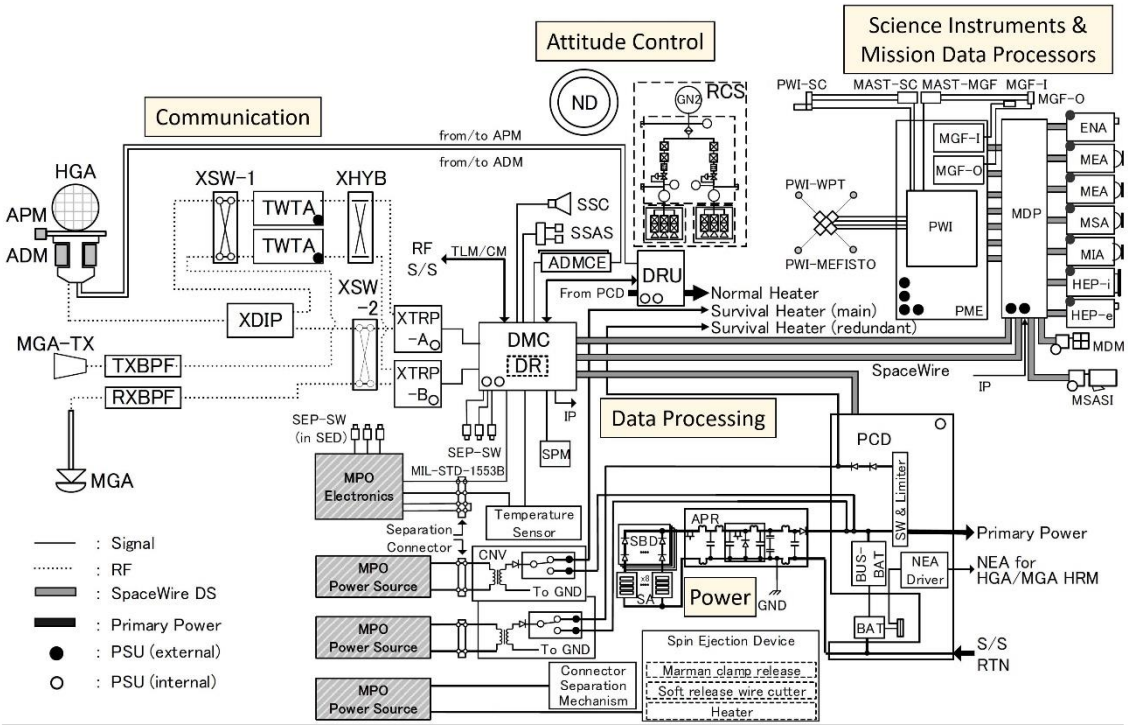

Figure 2: Block diagram of the Mio spacecraft system.

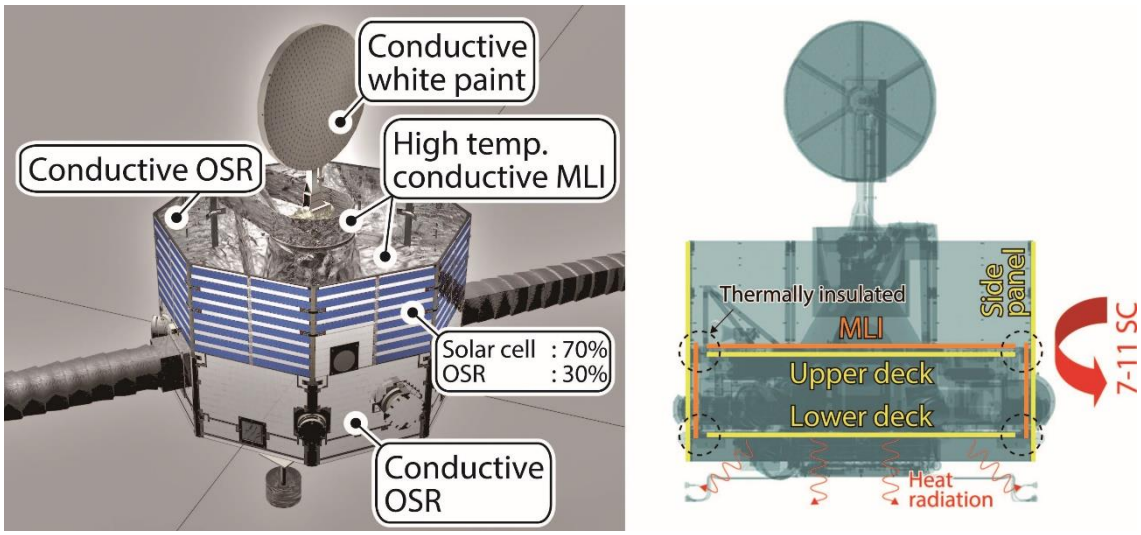

Figure 3: Thermal design of the Mio spacecraft.

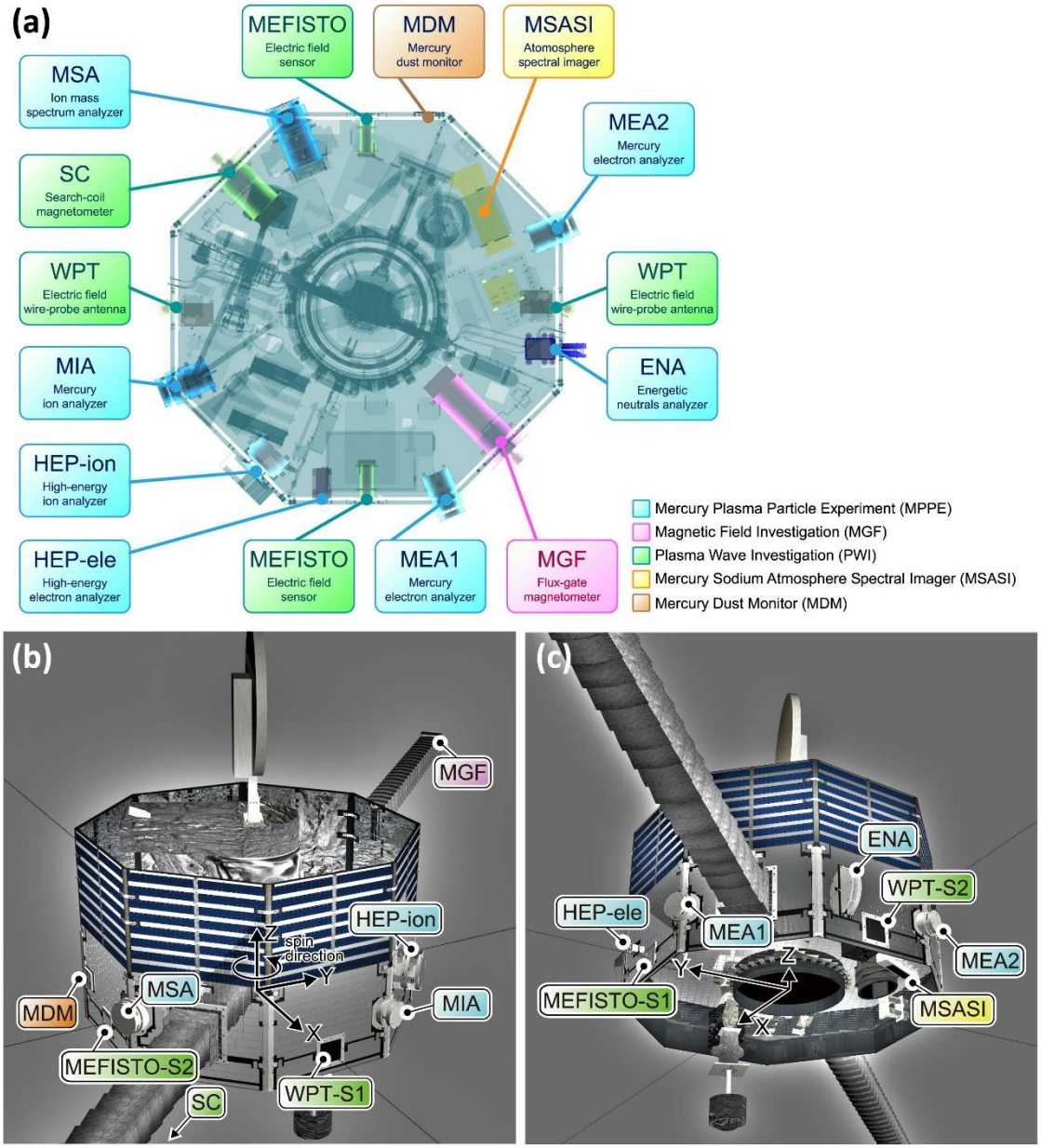

Figure 4: Schematic views of the Mio spacecraft identifying the science instruments. The location of each instrument and sensor is indicated from top (a), side (b), and bottom (c) views. The spacecraft coordinates and spin directions are indicated in (b) and (c).

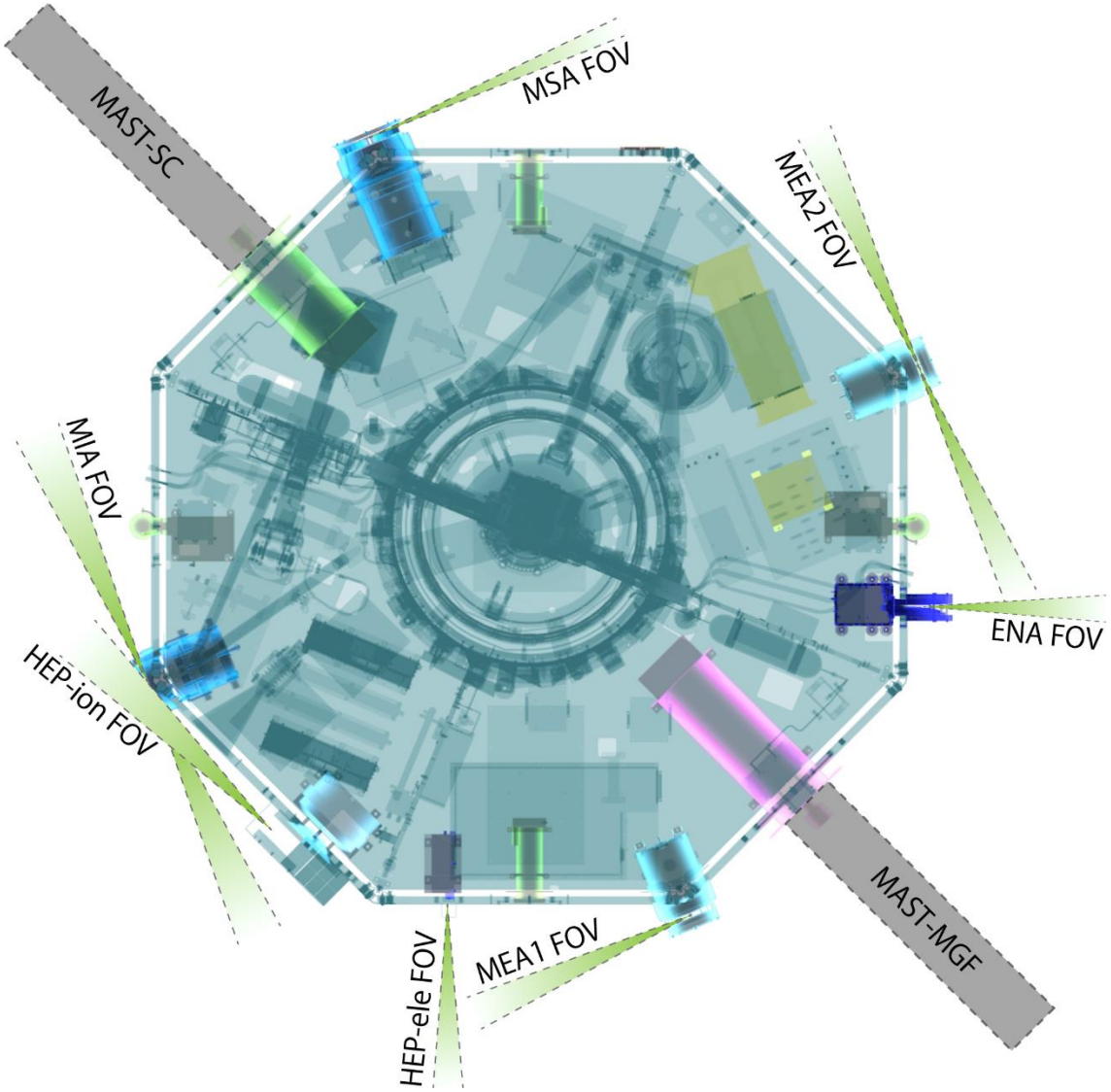

731

732 **Figure 5:** A schematic of the field of view of each MPPE sensor.

733

734

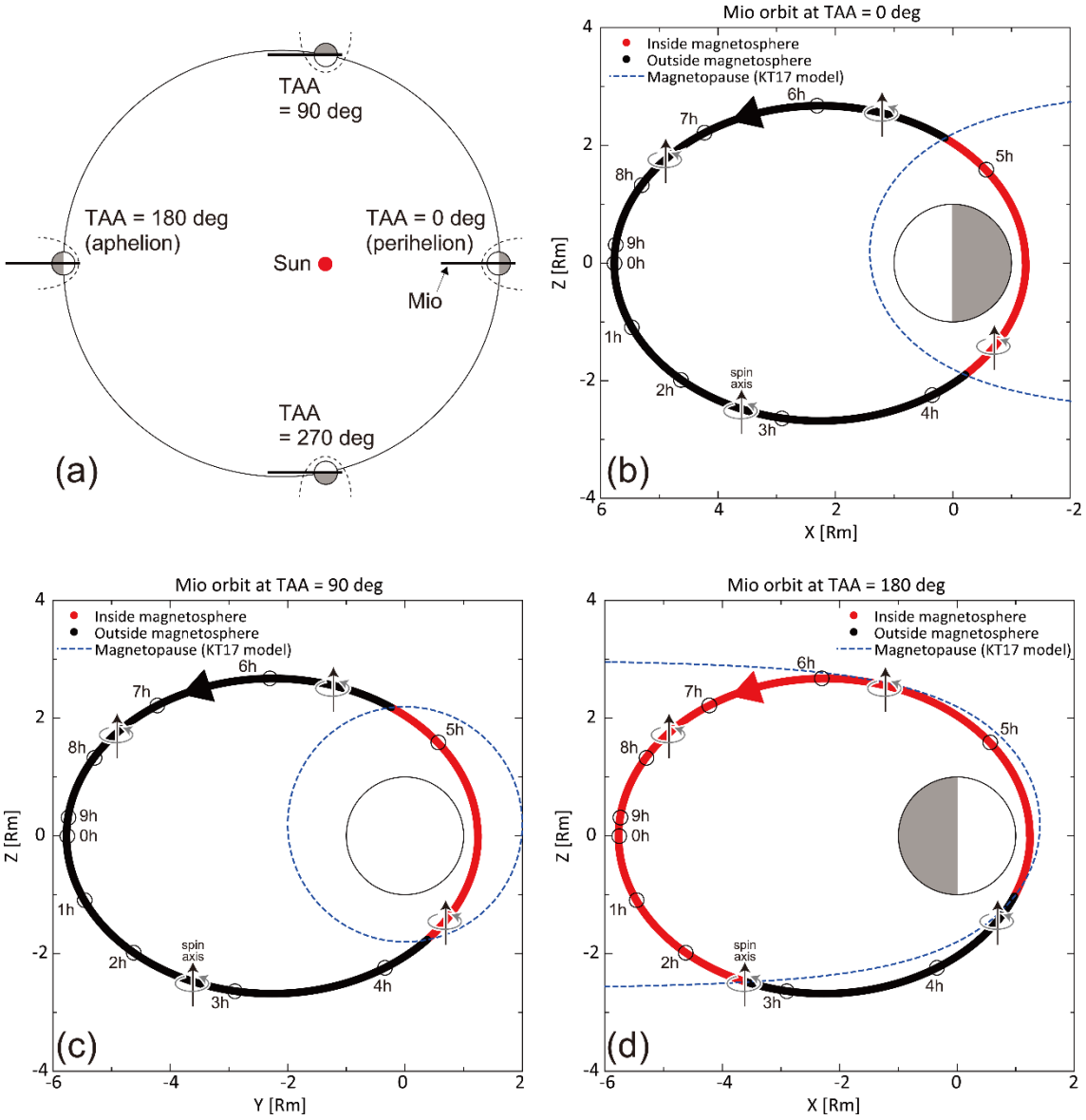

Figure 6: Orbits of Mio on Mercury's orbital plane (a) and the polar orbit at a true anomaly angle of 0° (b), 90° (c), and 180° (d). Mio's spin axis (almost same as Mio's z-axis shown in Figure 4) and spin direction are also shown in (b-d). The spacecraft locations every 1 hour from the periherm are indicated by black circles along the orbits in (b-d).

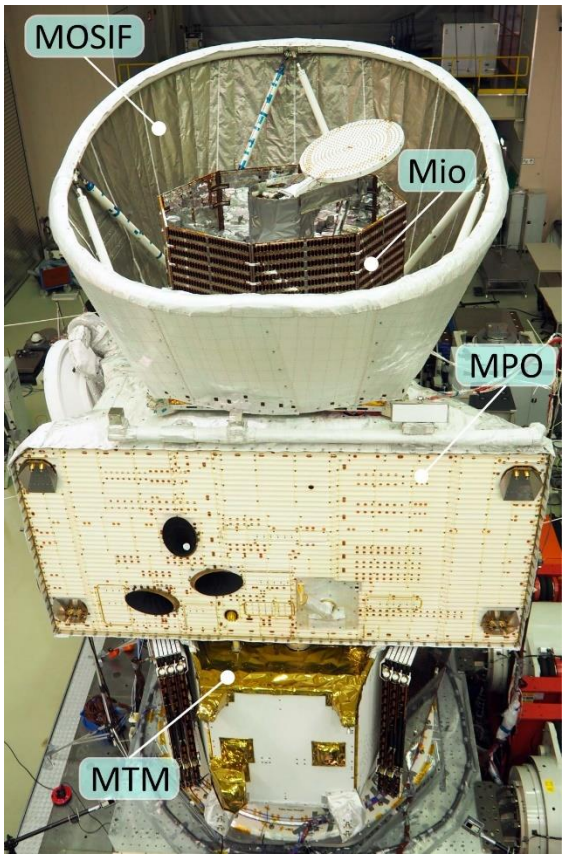

744

745 **Figure 7.** Configuration of the Mercury Composite Spacecraft (MCS) during vibration tests (same
746 condition as during launch). Mio is located at the top of MCS and surrounded by MOSIF.

747

748

749

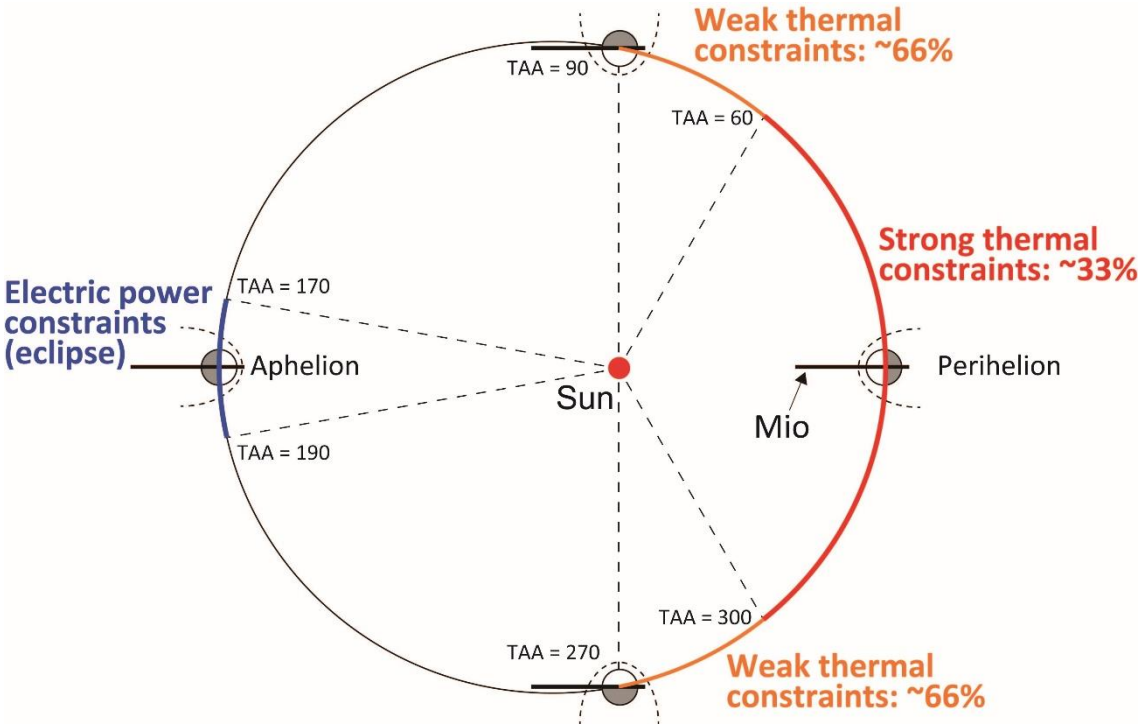

Figure 8. Schematic view of orbital phases with major operational constraints for Mio science operations. Science instruments will not be fully operable because of thermal constraints during the perihelion season and because of electrical power constraints in aphelion seasons.

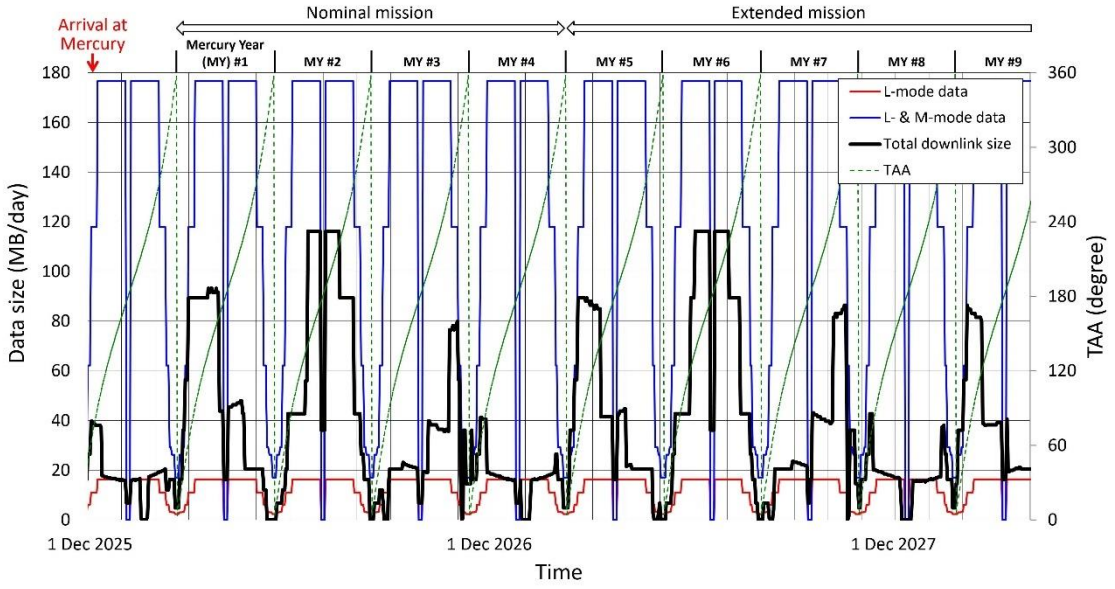

Figure 9. Expected temporal evolution of the data rates for total downlink size (black) and science data production with L-mode (red) and L- and M-mode (blue) during the nominal and extended mission phases. The green dashed line shows the true anomaly angle.

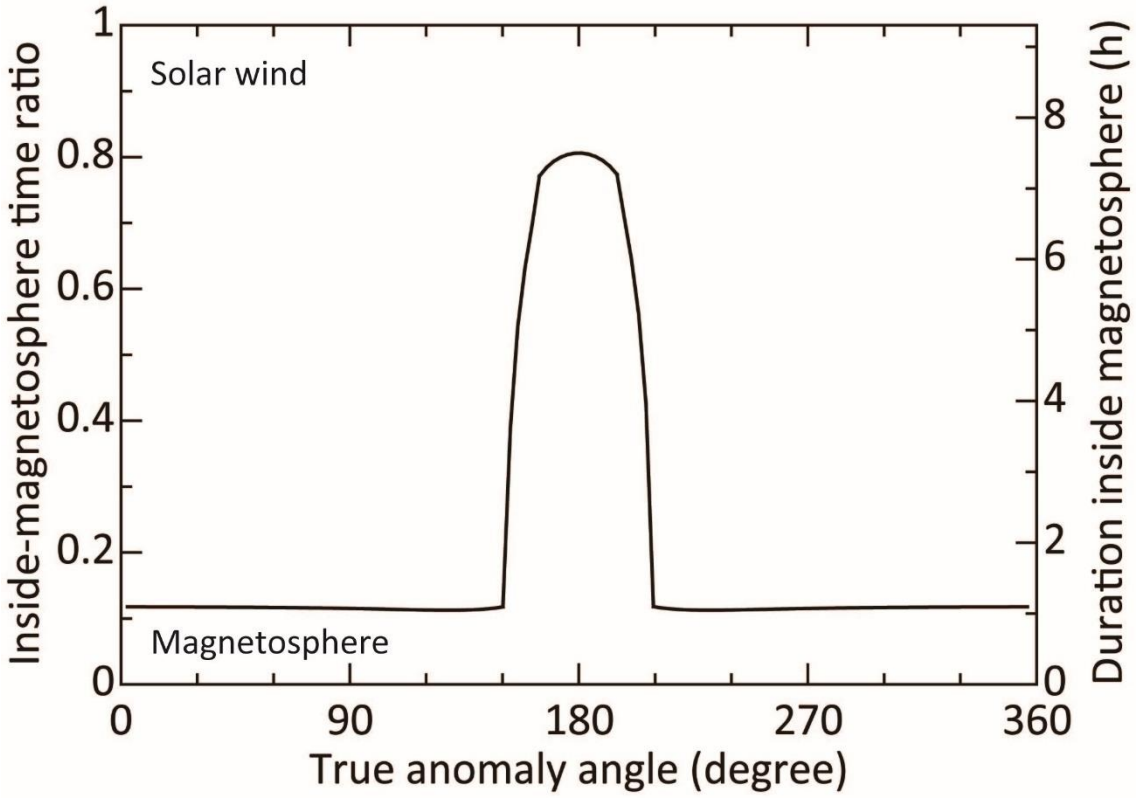

763

764 **Figure 10.** Seasonal variation of duration inside Mercury's magnetosphere in each spacecraft orbital
765 evolution.

766

767

768

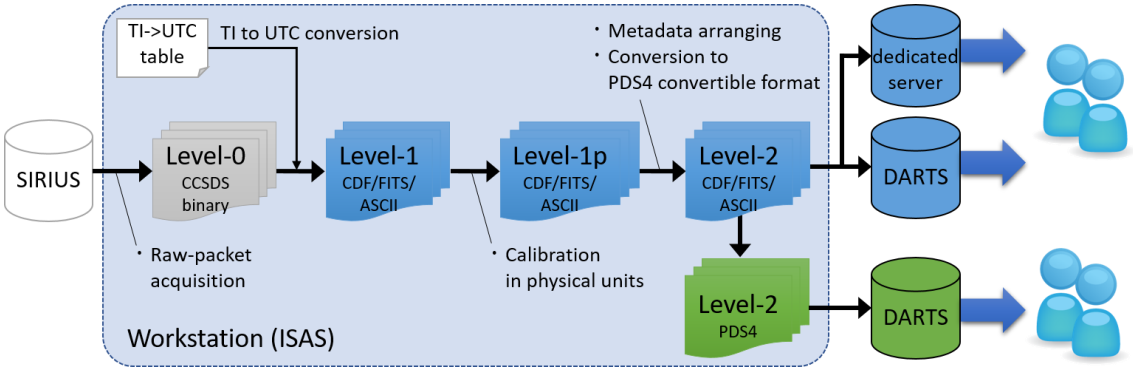

769

770 **Figure 11.** Outline of the science data pipeline.

771

772

773

774 **Table 1.** Success criteria of BepiColombo/Mio

	Minimum success	Full success	Extra success
Magnetic field	Confirm presence of the intrinsic magnetic field by MGF measurements for more than 88 Earth days (one Mercury year)	Perform global mapping (>80% coverage) with accuracy of <1 nT or <2% within one Earth year and obtain useful information to infer the origin of the magnetic field.	Separation between internal and external sources. Insight into planetary internal structure (collaboration with MPO)
Magnetosphere	Identify structure of the magnetosphere by either MPPE or PWI measurements for more than 88 Earth days.	Identify the effect of solar wind condition on magnetospheric structure from plasma density and temperature profiles with resolution of several hundred km within one Earth year. Understand the plasma dynamics with data of 10 s time resolution or higher.	Comparative magnetosphere theme: understanding common and unique features
Atmosphere	–––	Observe variation of the sodium exosphere for several hours with a few minutes time resolution, more than once in every quarter orbital position within one Earth year. Identify the effect of solar radiation and solar wind.	Understanding of source and loss mechanisms of the Mercury's atmosphere by collaboration with MPO and/or dust distribution information
Shock wave	–––	–––	*In-situ* observations of very high (Ma ~ 40) and/or low (Ma<1) Mach number shocks in the inner-heliosphere

775

776 **Table 2.** Specification of Mio

Shape	Octagonal shape within a 1.8 m diameter circle with two 5 m extendable mast and four 15 m (from tip to root) electric field antenna
Height	1.52 m (launch configuration) 2.66 m (observational configuration)
Mass	255 kg (including 3.7 kg N_2 gas) excluding 20 kg separation mechanism which remains on MMO sunshield interface (MOSIF)
Power (spin averaged)	≧271 W (periapsis at aphelion) ≧368 W (average at aphelion) ≧530 W (average at perihelion)
Designed mission life	One Earth year observation at the Mercury orbit
Thruster	6 × 0.4 N N_2 cold gas jet
Spin rate	15 rpm (4 s/spin)

777

778

779 **Table 3.** Summary of the science instruments onboard BepiColombo/Mio, compared with the
780 MESSENGER mission

Target	BepiColombo/Mio				MESSENGER	
Plasma	MPPE	MEA	Low-energy electrons	3 eV-26 keV	-	
		MIA	Low-energy ions	15 eV-29 keV	FIPS	50 eV-13 keV 1-40 amu/e
		MSA	Ion mass spectroscopy	1 eV-38 keV 1-60 amu/e m/Δm = 40 (<13 keV) m/Δm = 10 (>13 keV)		
		HEP-ion	High-energy ions	30 keV-1.5 MeV	EPS	25 keV-1 MeV
		HEP-ele	Hihg-energy electrons	30 keV-700 keV	EPS	25 keV-1 MeV
		ENA	Plasma imaging	10 eV-3.3 keV	-	
	MGF		Magnetic field	DC – 64 Hz (sampling) L: <0.25 Hz, M: 8 Hz	MAG	DC – 20 Hz (sampling)
	PWI		Electric field, plasma wave, radio wave	DC – 10 MHz (E) few – 640 kHz (B)	-	
Exosphere	MSASI		Na-exosphere image	Spatial resol.: 3-30 km R = 65000	MASCS	Spatial reol.: 25-800 km R = 1000
Dust	MDM		Dust environment	10s pg*km/s	-	

781
782
783
784

Table 4. Assumptions for downlink rate estimation of science telemetry data

Ground station	Misasa Deep Space Station (one station)
Coding	Turbo code
Geometrical constraints	Communication is available at Sun-Earth-Mercury angle > 3.0°
	Communication is available at the antenna elevation angle > 10°
Pass asignment for downlink	Everyday
	No conflicts with other spacecraft operations during Mio's visible pass
Spacecraft thermal constraint	Communication time = 2 h/day at TAA < 15°(~4 days)
	Communication time = 4 h/day at 15° < TAA < 45°(~10 days)
	Communication time = 6 h/day at 45° < TAA < 60°
Spacecraft electric power constraint	Communication time = 4 h/day at TAA > 175° (~3 days)
Ranging operations	1 h/week (50% data rate during RNG)
Station availability factor	85% (one Earth year average)
HK telemetry rate	64 s period (= ~0.5 kbps for real time and reproduct)

792 **Table 5.** Summary of averaged downlink rate for each period during Mercury orbit phase

Mercury year (MY)	Average DL rate (MB/day)	Period
0	18.4	24/11/2025–19/02/2026
1	47.1	20/02/2026–18/05/2026
2	62.9	19/05/2026–14/08/2026
3	26.6	15/08/2026–10/11/2026
4	16.9	11/11/2026–06/02/2027
5	40.5	07/02/2027–05/05/2027
6	65.1	06/05/2027–01/08/2027
7	31.6	02/08/2027–24/01/2028

793
794
795
796
797

798 **Table 6.** Definition of the science data level

Level	**Contents**	**Scope**	**File format**
Level-0	Raw-telemetry	Internal	CCSDS-Binary
Level-1	Observed data in instrument-dependent units	Internal	CDF, FITS, ASCII
Level-1p	Calibrated data in physical units	Internal	CDF, FITS, ASCII
Level-2	Calibrated data in physical units with appropriate metadata	Public	CDF, FITS, ASCII PDS4
Level-3	Processed data combining data from different instruments	Public	CDF, FITS, ASCII PDS4

799
800
801
802
803
804